Dyes and Pigments 90 (2011) 253–258

Contents lists available at ScienceDirect

Dyes and Pigments

journal homepage: www.elsevier.com/locate/dyepig

Improved thermal and photostability of an anthraquinone dye by intercalation in a zinc–aluminum layered double hydroxides host

Pinggui Tang, Yongjun Feng, Dianqing Li*

State Key Laboratory of Chemical Resource Engineering, Beijing University of Chemical Technology, Beijing 100029, PR China

ARTICLE INFO

Article history:
Received 19 September 2010
Received in revised form
12 January 2011
Accepted 14 January 2011
Available online 21 January 2011

Keywords:
Acid green 28
Intercalation
Anion-exchange
Layered double hydroxides
Thermostability
Photostability

ABSTRACT

Intercalation of the dianion of the anthraquinone dye Acid Green 28 (1,4-bis[(4-butylbenzene-2-sulphonate)amino]-5,8-dihydroxyanthraquinone) ($AG28^{2-}$) into a Zn_2Al–layered double hydroxides (LDH) has been carried out by an anion-exchange method in an effort to improve its thermostability and photostability. The interlayer distance of the LDH was 1.918 nm after reaction with $AG28^{2-}$ anions, confirming their intercalation into the interlayer galleries of the LDH host. Infrared spectroscopy and thermogravimetric analysis revealed the presence of host–guest interactions between LDH layers and $AG28^{2-}$ anions. The thermostability of AG28 as its sodium salt and Zn_2Al–AG28–LDH were compared by thermogravimetric–differential thermal analysis and UV–visible spectroscopy. It was found that the thermostability of AG28 was markedly improved by intercalation into the Zn_2Al–LDH host, whilst the photostability was enhanced slightly. In their composites with polyethylene, it was also found Zn_2Al–AG28–LDH possessed better thermostability and photostability than AG28 as its sodium salt.

1. Introduction

Pigments are widely used in various products such as paints, printing inks, plastics, fibers, rubbers, ceramics, enamels and glasses [1,2]. Pigments can be classified as inorganic pigments and organic pigments. Organic pigments show much brighter colors and are more widely used than inorganic pigments, especially as additives in plastics, fibers and rubbers. Unfortunately, however, organic pigments suffer from poor thermostability and photostability [3,4] and it is of practical importance to find ways of synthesizing pigments with higher thermostability and photostability.

Layered double hydroxides (LDH), also known as hydrotalcite-like compounds, is a class of anionic layered clays that can be represented by the general formula $[M^{2+}_{1-x}M^{3+}_{x}(OH)_2]^{x+}(A^{n-}_{x/n})\cdot mH_2O$, where M^{2+} and M^{3+} stand for various divalent and trivalent metal cations, respectively, in the host layers, the value of x ranges typically between 0.2 and 0.33, and A^{n-} represents the interlayer anions in the hydrated interlayer galleries [5–10]. Recently, LDHs have received considerable attention due to their anion-exchange capability. A variety of layered materials have been synthesized by different methods and LDHs have widespread applications as catalysts or catalyst precursors [11–14], adsorbents [15–17], anionic exchangers [18–20], in biochemistry [21–23], polymer additives [24,25] and as hybrid pigments[26–28].

Previous studies [26–28] have indicated that the thermostability of organic anions can be markedly improved after intercalation into the galleries of LDHs. Therefore pigments with enhanced thermostability and photostability may be synthesized by intercalating dye anions into the interlayer galleries of LDHs. Acid Green 28 (1,4-bis[(4-butylbenzene-2-sulphonate sodium salt)amino]-5,8-dihydroxyanthraquinone) (abbreviated as Na_2AG28) is a deep green dye. Its structural formula is shown in Fig. 1. It is widely used in the areas of textile dyeing and the coloring of plastics. Although the photostability of the dye is quite good, its thermostability is poor and thus it tends to fade in the course of polymer processing and its range of applications is severely restricted. In this work, intercalation of $AG28^{2-}$ anions into an LDH host was carried out by an ion-exchange method using a Zn_2Al–NO_3–LDH as a precursor, and the thermostability and photostability of the resulting intercalated material was compared with that of Na_2AG28.

2. Experimental section

2.1. Materials

NaOH, $Zn(NO_3)_2\cdot 6H_2O$, $Al(NO_3)_3\cdot 9H_2O$, HNO_3, ethanol and *N*,*N*–dimethyformamide (DMF) were A.R. grade reagents. Low-

* Corresponding author. Tel.: +86 10 64436992; fax: +86 10 64425385.
E-mail address: lidq@mail.buct.edu.cn (D. Li).

0143-7208/$ – see front matter © 2011 Elsevier Ltd. All rights reserved.
doi:10.1016/j.dyepig.2011.01.007

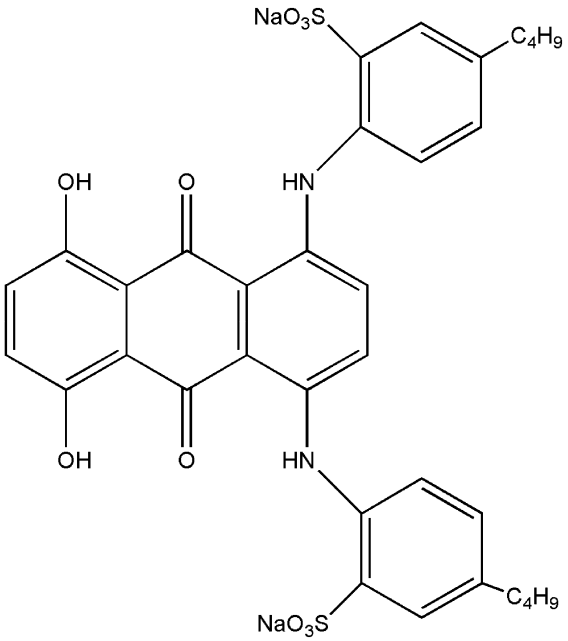

Fig. 1. The structural formula of Acid Green 28.

density polyethylene (PE, 1I2A-1) was purchased from Yanshan Petrochemical Company. Water used was deionized and decarbonated, with an electrical conductivity less than 10^{-6} S/cm. Acid Green 28 was a commercial product with a purity of 95% and was recrystallized three times in water before use.

2.2. Preparation of Zn_2Al–NO_3–LDH

The Zn_2Al–NO_3–LDH precursor was prepared by a method involving separate nucleation and aging steps (SNAS) [29] developed in our laboratory. $Zn(NO_3)_2 \cdot 6H_2O$ (71.39 g, 0.24 mol) and $Al(NO_3)_3 \cdot 9H_2O$ (45.02 g, 0.12 mol) were dissolved in water (300 mL) to form a mixed salt solution. NaOH (28.80 g, 0.72 mol) was dissolved in water (300 mL) to form an alkali solution. The two solutions were simultaneously added to a colloid mill with rotor speed set at 3000 revolutions per minute and mixed for 2 min. The resulting slurry was then aged at boiling temperature for 6 h under N_2 stream. The product was centrifuged and washed until the pH value of the centrifuged water was less than 8. A portion of the resulting filter cake was dried, showing that it contained 26.97 wt.% solid.

2.3. Synthesis of Zn_2Al–AG28–LDH

AG28 anion–intercalated LDH (Zn_2Al–AG28–LDH) was synthesized by an anion-exchange method using Zn_2Al–NO_3–LDH as precursor, similar to that already reported [28]. The intercalation was typically carried out as follows: A portion of the filter cake (9.2 g, containing ca. 7.3 mmol NO_3^-) was dispersed in 100 mL water under N_2 protection to form a white slurry and a solution of Na_2AG28 (21.6 g, molar ratio of $AG28^{2-}$ to NO_3^- = 4) in 300 mL water was added to the slurry under a nitrogen atmosphere. The concentration of AG28 in the final solution was about 0.097 M and the pH value was adjusted to 4.6 by adding 0.01 M HNO_3. The reaction was carried out under a nitrogen atmosphere at 100 °C for 96 h after the mixture was microwave treated for 1 h. The resulting precipitate was centrifuged at a speed of 4200 revolutions per minute and thoroughly washed with water and then further washed with DMF until the supernatant was nearly colorless. Finally, the product was washed twice with 100 mL ethanol and then dried at 100 °C for 24 h.

2.4. Characterization

X-ray diffraction (XRD) patterns were obtained using a Shimadzu XRD–6000 diffractometer with monochromatic Cu K_α radiation ($\lambda = 0.15406$ nm) operating at 40 kV and 30 mA. FT–IR spectra were collected on a Bruker Vector 22 infrared spectrophotometer using the KBr disk method with a weight ratio of sample/KBr of 1:100. Thermogravimetric–differential thermal analysis (TG–DTA) curves were recorded on a PCT–IA instrument in the temperature range 30–600 °C with a heating rate of 10 °C/min in flowing air. Diffuse reflectance UV–visible absorbance spectra were recorded using a Shimadzu UV-2501PC instrument with an integrating sphere attachment in the range 200–800 nm using $BaSO_4$ as the reference. Elemental analyses for metal elements and sulfur in the LDH powder were performed using an ICPS-7500 model inductively coupled plasma emission spectrometer (ICP–ES). Carbon and nitrogen analyses were carried out on Elementar vario EI Analyzer. The color difference (ΔE) of materials aged under UV light was determined in terms of CIE 1976 L*a*b* using a TC–P2A automatic colorimeter.

2.5. Thermo- and photostability of Zn_2Al–AG28–LDH/PE and Na_2AG28/PE

Na_2AG28 and Zn_2Al–AG28–LDH were separately incorporated into a polyethylene resin (PE) with the content of AG28 in the composite being 0.5 wt.% in each case. The Na_2AG28/PE and Zn_2Al–AG28–LDH/PE composite sheets of size 50 × 50 × 1 mm were molded and thermally aged in an oven at 100, 150 and 200 °C for 30 min. The color difference (ΔE) value was recorded after each heating step (A ΔE reading of 0 represents a perfect match and a value of 1 is supposed to represent the smallest variance the human eye can see, although the sensitivity of the human eye is not uniform across the visible spectrum). The Na_2AG28/PE and Zn_2Al–AG28–LDH/PE composite sheets were photoaged in a UV photoaging instrument (with an ultraviolet high pressure mercury lamp as UV light source, 1000 W power and wavelength range 250–380 nm) with a temperature control system. The color difference (ΔE) value was recorded after UV irradiation for 5 min. The process was repeated ten times, giving a total of 50 min accumulated exposure for each composite sheet.

3. Results and discussion

3.1. Structure of the samples

Fig. 2 shows the powder XRD patterns of Zn_2Al–NO_3–LDH, Na_2AG28 and Zn_2Al–AG28–LDH. The XRD pattern of the Zn_2Al–NO_3–LDH precursor (Fig. 2a) showed sharp, symmetrical peaks at low 2θ values corresponding to basal and higher order reflections. The basal spacing (d_{003}) of Zn_2Al–NO_3–LDH is 0.880 nm, which agrees well with the literature [28]. The diffraction pattern of Zn_2Al–AG28–LDH, shown in Fig. 2c, has a well-defined series of (*00l*) reflections at low 2θ values, corresponding to an expanded basal spacing of 1.918 nm, suggesting that $AG28^{2-}$ anions have been intercalated between the layers. The presence of the characteristic non-basal (*110*) reflection at 60.56° (2θ, d_{110} = 0.153 nm) [10–15], confirms that the LDH structure has been retained. Remind that (*110*) and (*113*) Bragg reflections are overlapped for most of organic anions intercalated LDHs [30]. Here, we separate both peaks using Gaussian fitting function as shown in the inset graph. The diffraction pattern of

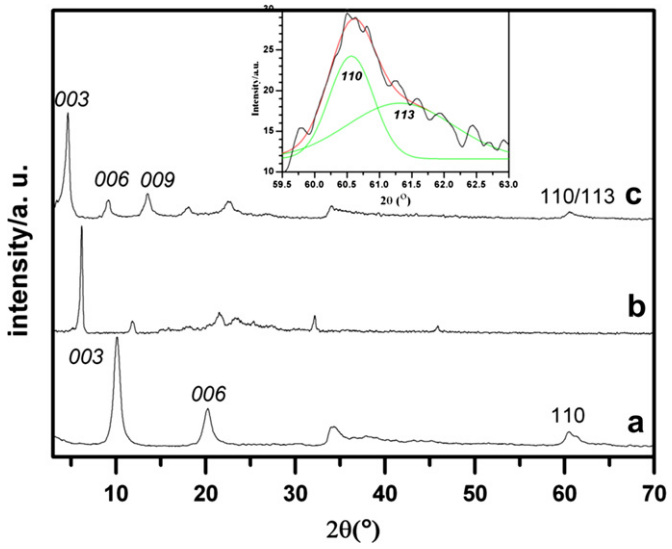

Fig. 2. XRD patterns of the $Zn_2Al–NO_3–LDH$ precursor (a), Na_2AG28 (b) and $Zn_2Al–AG28–LDH$ (c). The inset presents the (c) in the range of 2-theta from 59.5° to 63° and the corresponding Gaussian fitting.

the product (Fig. 2c) contains no peaks characteristic of either the $Zn_2Al–NO_3–LDH$ (Fig. 2a) or the Na_2AG28 precursors (Fig. 2b), suggesting that the anion-exchange reaction has gone to completion. The unit cell parameters a and c of $Zn_2Al–AG28–LDH$ can be calculated from the positions of the (*110*) and (*003*) reflections: $a = 2d_{110} = 0.306$ nm and $c = 3d_{003} = 5.754$ nm, respectively.

3.2. FT–IR analysis

Fig. 3 displays the FT–IR spectra of $Zn_2Al–NO_3–LDH$, Na_2AG28 and $Zn_2Al–AG28–LDH$ in the 4000–400 cm^{-1} wavenumber range. In the spectrum of the $Zn_2Al–NO_3–LDH$ precursor, displayed in Fig. 3a, the broad absorption band centered at around 3500 cm^{-1} is assigned to the stretching vibrations of the hydroxyl groups of LDH layers and interlayer water molecules. The strong band at 1384 cm^{-1} is the characteristic absorption of the intercalated nitrate anion. The absorption band at 609 cm^{-1} is ascribed to the M–OH bending vibration and the absorption band at 427 cm^{-1} is attributed to the lattice vibrations of O–M–O [31].

As shown in Fig. 3b, in the spectrum of Na_2AG28, a broad band attributed to the OH stretching vibration overlapping with the NH stretching vibration can be observed at around 3404 cm^{-1}. The rocking vibration band of the OH group can be also observed at 628 cm^{-1}. The absorption bands at 2953, 2926, 2868, and 2857 cm^{-1} is assigned to the stretching vibrations of the alkyl groups. The absorption bands at 1599, 1565 and 1499 cm^{-1} correspond to the characteristic vibration bands of phenyl groups. The band at 827 cm^{-1} is attributed to the C–H deformation vibrations

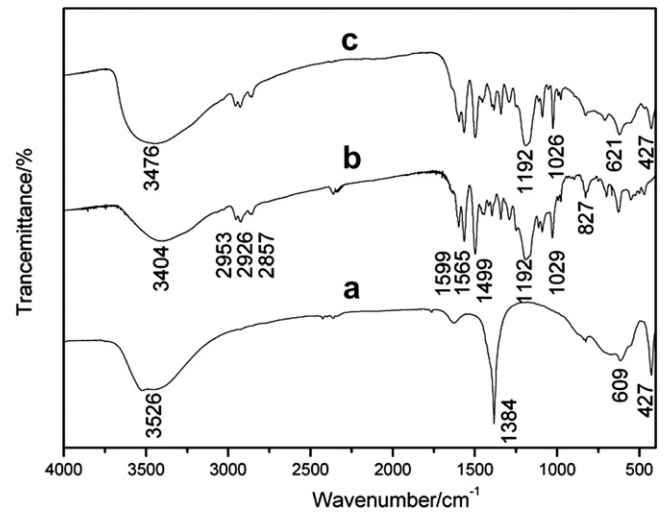

Fig. 3. FT–IR spectra of the $Zn_2Al–NO_3–LDH$ precursor (a), Na_2AG28 (b) and $Zn_2Al–AG28–LDH$ (c).

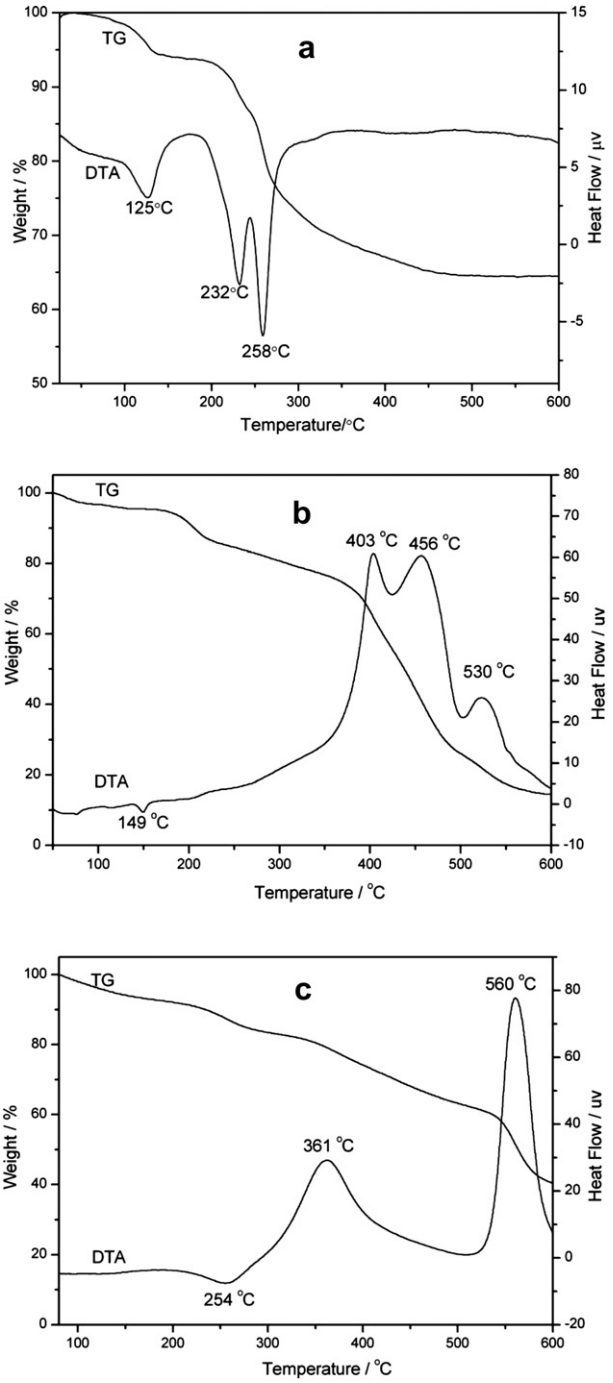

Fig. 4. TG–DTA curves of $Zn_2Al–NO_3–LDH$ precursor (a), Na_2AG28 (b) and $Zn_2Al–AG28–LDH$ (c).

Table 1
Chemical compositions of Zn_2Al-NO_3-LDH and $Zn_2Al-AG28-LDH$.

Samples	Zn	Al	N	S	C	Formula
	Found (calc.)	Found (calc.)	Found (calc.)	Found (calc.)	Found (calc.)	
Zn_2Al-NO_3-LDH	37.37	7.98	4.14			$Zn_{0.659}Al_{0.341}(OH)_2(NO_3)_{0.341}\cdot 0.45H_2O$
	37.29	7.97	4.13			
$Zn_2Al-AG28-LDH$	19.87	4.16	2.05	4.93	31.67	$Zn_{0.664}Al_{0.336}(OH)_2(AG28)_{0.168}\cdot 0.73H_2O$
	20.10	4.20	2.18	4.98	31.73	

out of the plane of the aromatic ring. The asymmetric and symmetric stretching vibrations of the $-SO_3^-$ group appear at 1192 and 1029 cm^{-1}, respectively [32].

Fig. 3c depicts the FT–IR spectrum of $Zn_2Al-AG28-LDH$. The IR spectrum demonstrates the characteristic features of LDH-like materials together with the characteristic frequencies associated with the presence of $AG28^{2-}$ anions. The broad band centered at around 3476 cm^{-1} is due to the OH stretching vibration of interlayer water, hydroxyl groups on the layers and $AG28^{2-}$ anions and the NH stretching vibration of $AG28^{2-}$ anions. The characteristic absorption bands of the alkyl groups are observed at 2955, 2929, 2869 and 2858 cm^{-1}. The absorption bands at 1599, 1566 and 1499 cm^{-1} is assigned to the vibration of phenyl groups. The absorption bands of the asymmetric and symmetric stretching vibrations of the $-SO_3^-$ group appear at 1192 and 1026 cm^{-1}, respectively. The characteristic absorption bands of LDH materials are observed in the low-frequency region. The absorption band at 621 cm^{-1} is ascribed to the M–OH bending vibration and the absorption band at 427 cm^{-1} is attributed to the lattice vibrations of O–M–O [31]. There is slight shifts in the positions of the absorption bands of the symmetric stretching vibrations of the $-SO_3^-$ group and the bending vibration of M–OH, compared with the corresponding values in the precursors, which can be ascribed to hydrogen bonding interactions between $AG28^{2-}$ anions and hydroxyl groups on the layers.

The XRD and FT–IR results confirm the formation of a new organic–inorganic hybrid pigment consisting of an LDH intercalated with $AG28^{2-}$ anions.

3.3. TG–DTA analysis

Fig. 4 depicts the TG–DTA curves of the Zn_2Al-NO_3-LDH precursor, Na_2AG28 and $Zn_2Al-AG28-LDH$. We observe three endothermic peaks centered at 125 °C, 232 °C and 258 °C in the DTA curve of Zn_2Al-NO_3-LDH in Fig. 4a. The TG curve has three corresponding weight loss stages. The first and the second stages can be attributed to the release of the interlayer water and the dehydroxylation of the Zn_2Al-NO_3-LDH basal layers, respectively. The third large weight loss stage in the temperature region 244–500 °C is due to further dehydroxylation of the layers and the decomposition of the nitrate anions [31].

The TG curve of Na_2AG28 (Fig. 4b) demonstrates three weight loss stages. The first weight loss stage below 100 °C corresponds to the removal of physically adsorbed water. The second weight loss stage from 160 to 250 °C corresponds to the oxidative thermal decomposition of the organic anion; accordingly there is a small exothermic peak in the DTA curve. The third weight loss stage from 250 to 600 °C can be attributed to the combustion of the residue, and the DTA curve showed two strong exothermic peaks at 403 and 456 °C and a weak exothermic peak at 530 °C.

As revealed in Fig. 4c, the TG–DTA curve of $Zn_2Al-AG28-LDH$ is very different from that of Na_2AG28, although the TG curve also showed three mass loss stages. The first mass loss stage below 300 °C can be assigned to the loss of adsorbed water, and the removal of interlayer water as well as the dehydroxylation of the $Zn_2Al-AG28-LDH$ layers. Accordingly, the DTA curve displays an endothermic peak at around 254 °C corresponding to the dehydroxylation. The second mass loss stage between 300 and 500 °C can be attributed to the oxidative thermal decomposition of the $AG28^{2-}$ anions in the interlayer galleries of $Zn_2Al-LDH$ with a broad exothermic peak centered at 361 °C in the DTA curve. The third mass loss stage from 500 to 600 °C can be attributed to the combustion of the residue of $AG28^{2-}$ anions, and the DTA curve shows a strong exothermic peak at 560 °C. Comparing the DTA curves of Na_2AG28 with $Zn_2Al-AG28-LDH$, one sees that the temperature for oxidative thermal decomposition of $AG28^{2-}$ anions in the interlayer of $Zn_2Al-AG28-LDH$ is much higher than that for Na_2AG28. Possibly, this is due to the presence of a strongly hydrogen bonded network in the interlayer galleries involving the hydroxyl groups of the layers and the $AG28^{2-}$ anions. The differences between the TG–DTA curves for Na_2AG28 and $Zn_2Al-AG28-LDH$, together with the differences between their infrared spectra, discussed above, are consistent with there being a supramolecular structure with significant host–guest interactions in $Zn_2Al-AG28-LDH$ which increases the thermal decomposition temperature of $AG28^{2-}$ anions.

3.4. Elemental analysis

Elemental analysis data for $Zn_2Al-AG28-LDH$ are listed in Table 1. The analytical data confirm that the $AG28^{2-}$ anions have been intercalated into the interlayer galleries of LDH. The amount of crystal water can be calculated from the magnitude of the first weight loss step below 150 °C in the TG curves for Zn_2Al-NO_3-LDH (7%) and $Zn_2Al-AG28-LDH$ (6%). The Zn^{2+}/Al^{3+} molar ratio in $Zn_2Al-AG28-LDH$ (1.97) is almost the same as that of the Zn_2Al-NO_3-LDH precursor (1.93), indicating that the layers remained intact during the intercalation process.

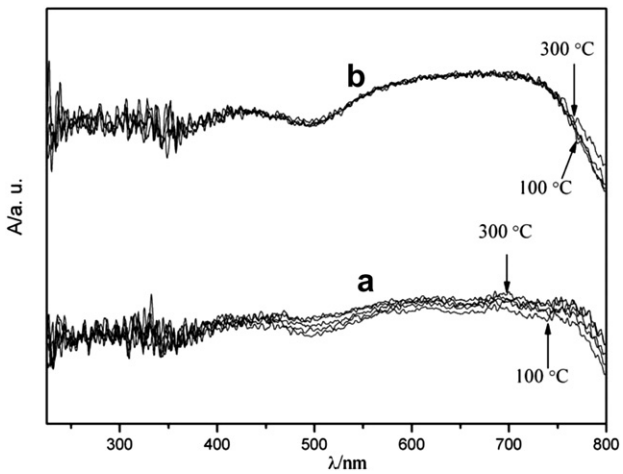

Fig. 5. UV–visible spectra of Na_2AG28 (a) and $Zn_2Al-AG28-LDH$ (b) after thermal aging at different temperatures.

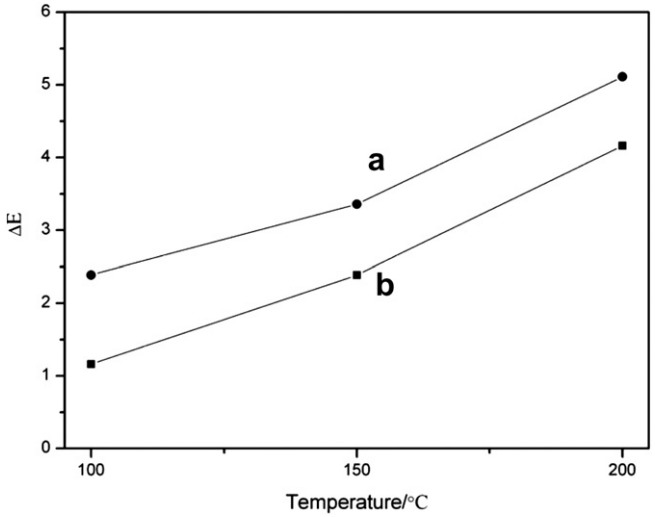

Fig. 6. Color difference (ΔE) values for Na_2AG28/PE (a) and Zn_2Al–AG28–LDH/PE (b) composite sheets after thermal aging at different temperatures.

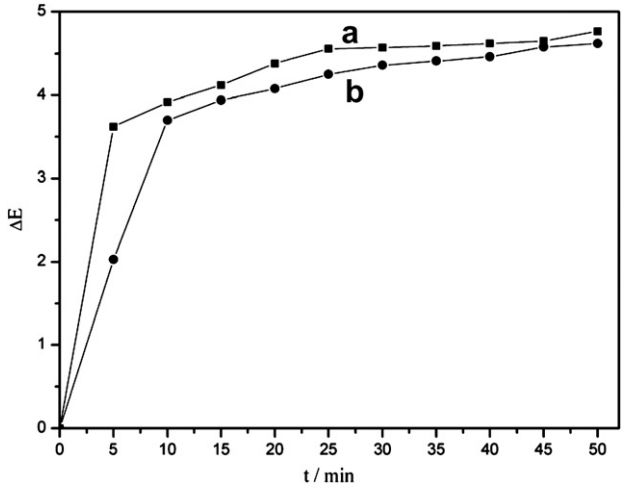

Fig. 8. Color difference (ΔE) values for Na_2AG28/PE (a) and Zn_2Al–AG28–LDH/PE (b) composite sheets after UV aging for different times.

3.5. Thermostability of samples

Fig. 5 demonstrates the diffuse reflectance UV–visible spectra of powdered samples of Na_2AG28 and Zn_2Al–AG28–LDH after heated in an oven at 100, 150, 200, 250, and 300 °C for 30 min. The absorption spectrum of Na_2AG28 shows significant changes on heating at temperatures above 150 °C, especially in the range from 400 to 800 nm. With increasing temperature, the changes in the spectra become much more marked. This indicates that Na_2AG28 begins to decompose at 150 °C and it is further decomposed as the temperature is increased above 150 °C. In the case of Zn_2Al–AG28–LDH, however, there is no significant change in the spectra after heating below 250 °C. Even after heating at 300 °C, the spectrum changes only slightly in the range from 700 to 800 nm, suggesting that Zn_2Al–AG28–LDH can tolerate higher temperatures than Na_2AG28. These results conclusively demonstrate that the thermostability of the $AG28^{2-}$ anions is enhanced after intercalation into the interlayer galleries of the Zn_2Al–LDH.

Na_2AG28 and Zn_2Al–AG28–LDH were separately incorporated in a polyethylene (PE) resin with the content of AG28 in the composite being 0.5 wt.%. It should be pointed out that the color of Na_2AG28 began to change during the preparation of the Na_2AG28/PE composite, suggesting Na_2AG28 started to decompose during the course of incorporation. However, there was no color change in the case of Zn_2Al–AG28–LDH. Na_2AG28/PE and Zn_2Al–AG28–LDH/PE composite sheets were heated in an oven at 100, 150 and 200 °C for 30 min and the ΔE values were recorded after each treatment. The ΔE values for Na_2AG28/PE, see Fig. 6, are larger than those for Zn_2Al–AG28–LDH/PE after thermal aging at the same temperatures, suggesting that the Zn_2Al–AG28–LDH/PE composite has better thermostability than the Na_2AG28/PE composite.

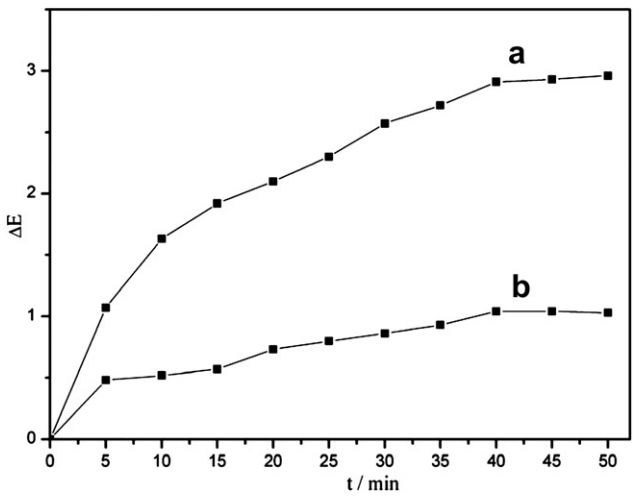

Fig. 7. Color difference (ΔE) values for Na_2AG28 (a) and Zn_2Al–AG28–LDH (b) after UV aging for different times.

3.6. Photostability of samples

Powdered samples of Na_2AG28 and Zn_2Al–AG28–LDH were photoaged in a UV photoaging instrument equipped with a temperature control system. The color difference (ΔE) values of the irradiated samples (Fig. 7) were measured using the CIE 1976 L*a*b* method every 5 min up to a total exposure time of 50 min. The ΔE values for Na_2AG28 are considerably larger than those for Zn_2Al–AG28–LDH after irradiation for the same times. The ΔE value of Na_2AG28 exceeds 2.9 after aging for 50 min, whereas the ΔE value for Zn_2Al–AG28–LDH is less than 1.1. These values suggest that the photostability of $AG28^{2-}$ anions is improved by intercalation into the interlayer galleries of Zn_2Al–LDH. This is possibly due to the presence of the strongly hydrogen bonded network in the interlayer galleries between the hydroxyl groups of the layers and the $AG28^{2-}$ anions.

Na_2AG28/PE and Zn_2Al–AG28–LDH/PE composite sheets of size 50 × 50 × 1 mm were molded and photoaged in the same UV photoaging instrument. The color difference (ΔE) values of Na_2AG28/PE and Zn_2Al–AG28–LDH/PE composite sheets after UV aging for different times are depicted in Fig. 8. It can be seen that the ΔE values for Na_2AG28/PE are larger than those for Zn_2Al–AG28–LDH/PE after photoaging for the same times, indicating that the photostability of AG28 used as a pigment in PE resin can be improved by intercalating into the galleries of Zn_2Al–LDH.

4. Conclusions

An $AG28^{2-}$ anion-pillared LDH has been successfully prepared to produce organic–inorganic composite pigment by an anion-exchange method. The intercalation of dye anions into the

interlayer of Zn_2Al–LDH significantly improves thermal- and photostability of dye anions due to the interaction between the brucite-like layer and the guest anions. It is a promising way to design and develop novel pigments with special thermostability and photostability for practical applications.

Acknowledgments

This work was supported by National Natural Science Foundation (Grant No.: 20971013), the Program for Changjiang Scholars and Innovative Research Teams in Universities (Project No.: IRT0406) and the 111 Project (Project No.: B07004).

References

[1] Visinescu D, Paraschiv C, Ianculescu A, Jurca B, Vasile B, Carp O. The environmentally benign synthesis of nanosized $Co_xZn_{1-x}Al_2O_4$ blue pigments. Dyes and Pigments 2010;87:125–31.
[2] Vishnu VS, George G, Divya V, Reddy MLP. Synthesis and characterization of new environmentally benign tantalum-doped $Ce_{0.8}Zr_{0.2}O_2$ yellow pigments: applications in coloring of plastics. Dyes and Pigments 2009;82:53–7.
[3] Binkowski S, Jesionowski T, Krysztafkiewicz A. Preparation of pigments on modified precipitated silicas. Dyes and Pigments 2000;47:247–57.
[4] Thetford D, Chorlton AP. Investigation of vat dyes as potential high performance pigments. Dyes and Pigments 2004;61:49–62.
[5] Thomas N, Kumar GP, Rajamathi M. Synthesis and intracrystalline oxidation of nitrite-intercalated layered double hydroxides. Journal of SolidState Chemistry 2009;182:592–6.
[6] Hosni K, Srasra E. Simplified synthesis of layered double hydroxide using a natural source of magnesium. Applied Clay Science 2009;43:415–9.
[7] Arai Y, Ogawa M. Preparation of Co–Al layered double hydroxides by the hydrothermal urea method for controlled particle size. Applied Clay Science 2009;42:601–4.
[8] Huang S, Cen X, Peng H, Guo S, Wang W, Liu T. Heterogeneous ultrathin films of poly(vinyl alcohol)/layered double hydroxide and montmorillonite nanosheets via layer-by-layer assembly. Journal of Physical Chemistry B 2009;113:15225–30.
[9] Johnsen RE, Norby P. A structural study of stacking disorder in the decomposition oxide of MgAl layered double hydroxide: a DIFFaX+ analysis. Journal of Physical Chemistry C 2009;113:19061–6.
[10] Shi W, Wei M, Lu J, Evans DG, Duan X. Studies on the orientation and polarized photoluminescence of α–naphthalene acetate in the layered double hydroxide matrix. Journal of Physical Chemistry C 2009;113:12888–96.
[11] Wei M, Zhang X, Evans DG, Duan X, Li X, Chen H. Rh-TPPTS intercalated layered double hydroxides as hydroformylation catalyst. AIChE Journal 2007;53:2916–24.
[12] Gao L, Tang Y, Xue Q, Liu Y, Lu Y. Hydrotalcite-like compounds derived CuZnAl oxide catalysts for aerobic oxidative removal of gasoline-range organo-sulfur compounds. Energy and Fuels 2009;23:624–30.
[13] Sels BF, De Vos DE, Buntinx M, Jacobs PA. Transition metal anion exchanged layered double hydroxides as a bioinspired model of vanadium bromoperoxidase. Journal of Catalysis 2003;216:288–97.
[14] Kantam ML, Laha S, Yadav J, Likhar PR, Sreedhar B, Jha S, et al. An efficient copper–aluminum hydrotalcite catalyst for asymmetric hydrosilylation of ketones at room temperature. Organic Letters 2008;10:2979–82.
[15] Zhu MX, Li YP, Xie M, Xin HZ. Sorption of an anionic dye by uncalcined and calcined layered double hydroxides: a case study. Journal of Hazardous Materials 2005;120:163–71.
[16] Inacio J, Taviot-Guého C, Forano C, Besse JP. Adsorption of MCPA pesticide by MgAl-layered double hydroxides. Applied Clay Science 2001;18:255–64.
[17] Vreysen S, Maes A. Adsorption mechanism of humic and fulvic acid onto Mg/Al layered double hydroxides. Applied Clay Science 2008;38:237–49.
[18] Jobbagy M, Regazzoni AE. Anion-exchange equilibrium and phase segregation in hydrotalcite systems: intercalation of hexacyanoferrate(III) ions. Journal of Physical Chemistry B 2005;109:389–93.
[19] Bontchev RP, Liu S, Krumhansl JL, Voigt J, Nenoff TM. Synthesis, characterization, and ion exchange properties of hydrotalcite $Mg_6Al_2(OH)_{16}(A)_x(A')_{2-x}\cdot 4H_2O$ (A, A′ = Cl^-, Br^-, I^-, and NO_3^-, $2 > x > 0$) derivatives. Chemistry of Materials 2003;15:3669–75.
[20] Feng YJ, Williams GR, Leroux F, Taviot-Guého C, O'Hare D. Selective anion-exchange properties of second-stage layered double hydroxide hetero structures. Chemistry of Materials 2006;18:4312–8.
[21] Desigaux L, Belkacem MB, Richard P, Cellier J, Léone P, Leroux F, et al. Self-assembly and characterization of layered double hydroxide/DNA hybrids. Nano Letters 2006;6:199–204.
[22] Yang QZ, Yang J, Zhang CK. Synthesis and properties of cordycepin intercalates of Mg–Al–nitrate layered double hydroxides. International Journal of Pharmaceutics 2006;326:148–52.
[23] Li B, He J, Evans DG, Duan X. Inorganic layered double hydroxides as a drug delivery system-intercalation and in vitro release of fenbufen. Applied Clay Science 2004;27:199–207.
[24] Fischer H. Polymer nanocomposites: from fundamental research to specific applications. Materials Science and Engineering C 2003;23:763–72.
[25] Li DQ, Tuo ZJ, Evans DG, Duan X. Preparation of 5-benzotriazolyl-4-hydroxy-3-sec-Butylbenzenesulfonate anion-intercalated layered double hydroxide and its photostabilizing effect on polypropylene. Journal of Solid State Chemistry 2006;179:3114–20.
[26] Hwang SH, Jung SC, Yoon SM, Kim DK. Preparation and characterization of dye-intercalated Zn–Al-layered double hydroxide and its surface modification by silica coating. Journal of Solid State Chemistry 2008;69:1061–5.
[27] Tian Y, Wang G, Li F, Evans DG. Synthesis and thermo-optical stability of o-methyl red-intercalated Ni–Fe layered double hydroxide material. Materials Letters 2007;61:1662–6.
[28] Tang P, Xu X, Lin Y, Li D. Enhancement of the thermo- and photo-stability of an anionic dye by intercalation in a zinc–aluminum layered double hydroxide host. Industrial and Engineering Chemistry Research 2008;47:2478–83.
[29] Zhao Y, Li F, Zhang R, Evans DG, Duan X. Preparation of layered double-hydroxide nanomaterials with a uniform crystallite size using a new method involving separate nucleation and aging steps. Chemistry of Materials 2002;14:4286–91.
[30] Kaćfunkovać E, Taviot-Guećho C, Bezdicka P, Klementovać M, Kovaćr P, Kubaćt P, et al. Porphyrins intercalated in Zn/Al and Mg/Al layered double hydroxides: properties and structural arrangement. Chemistry of Materials 2010;22(8):2481–90.
[31] Xu ZP, Zeng HC. Decomposition pathways of hydrotalcite-like compounds $Mg_{1-x}Al_x(OH)_2(NO_3)_x\cdot nH_2O$ as a continuous function of nitrate anions. Chemistry of Materials 2001;13:4564–72.
[32] Zhang H, Wen X, Wang Y. Synthesis and characterization of sulfate and dodecylbenzenesulfonate intercalated zinc–iron layered double hydroxides by one-step coprecipitation route. Journal of SolidState Chemistry 2007;180:1636–47.